Modification of Azithromycin to Mitigate its Arrest of Autophagy

Authors:

Ryan D Quarrington[1,2], Sylvia A Sapula[3], Susan E Lester[4], Matthew M Miller[5], Vesna M Kos[6], Benjamin T Kopp[7,8,9], Hubertus PA Jersmann[1,10], Anton Blencowe [11]*, Eugene Roscioli[1,10,12]*‡.

Affiliations

[1]Adelaide Medical School, University of Adelaide, Adelaide, South Australia, Australia.

[2]Centre for Orthopedic & Trauma Research, Faculty of Health and Medical Sciences, The University of Adelaide, Adelaide, South Australia, Australia.

[3]Health and Biomedical Innovation, UniSA Clinical and Health Sciences, University of South Australia, Adelaide, South Australia, Australia.

[4]Department of Rheumatology, The Queen Elizabeth Hospital, Adelaide, South Australia, Australia.

[5]Department of Premier and Cabinet, Lot Fourteen, Adelaide, South Australia, Australia.

[6]Department of Physiology and Pharmacology, Karolinska Institutet, Stockholm, Sweden.

[7]Center for Microbial Pathogenesis, The Abigail Wexner Research Institute at Nationwide Children's Hospital, Columbus, OH, USA.

[8]Division of Pulmonary Medicine, Nationwide Children's Hospital, Columbus, OH, USA.

[9]Infectious Disease Institute, The Ohio State University, Columbus, OH, USA.

[10]Department of Thoracic Medicine, Royal Adelaide Hospital, Adelaide, South Australia, Australia.

[11]Applied Chemistry and Translational (ACTB) Group, Centre for Pharmaceutical Innovation (CPI), UniSA Clinical and Health Sciences, University of South Australia, Adelaide, Australia.

[12]Centre for Cancer Biology, SA Pathology and University of South Australia, Adelaide, South Australia, Australia.

* Authors contributed equally

‡ Correspondence: Eugene Roscioli
Adelaide Health and Medical Science
Building, Corner of North Terrace and
George St, Adelaide 5005, South
Australia, Australia
Tel +61 8 8313 7088
Email: Eugene.Roscioli@adelaide.edu.au

Abstract:

Aims/hypothesis: Autophagy plays a critical role in the survival and microbial clearance functions of airway epithelial cells (**AEC**). Contrary to the known roles of azithromycin (**AZM**) in promoting microbial clearance, our preliminary evidence suggests that AZM inhibits autophagy in mammalian cells - an effect that could potentially promote bacterial residency in chronic respiratory diseases. Here we investigate the structure-activity relationship of AZM vs an AZM derivative (**AZM-[O]**), to mitigate the off-target arrest of autophagy.

Method: Participant-derived COPD vs control airway biopsies were assessed for intrinsic defects in autophagy-gene activity using an qRT-PCR array. For *in vitro* studies, the 16HBE14o- AEC line and Western blot were used to assess macrolide vs autophagy structure-activity relationships, and autophagic flux by quantifying the protein abundance of LC3B-II vs Sequestosome-1. Subsequent assessments of antimicrobial activity were conducted using an *E coli* model and the minimum inhibitory concentration method. Immunomodulatory outcomes were assessed by quantifying the secretion of IL-6 in an LPS-stimulated THP-1 macrophage model.

Results: Signatures of transcript-abundance showed an overall reduction in autophagy gene activity in COPD vs control biopsies. AZM significantly inhibited autophagic flux, evidenced by the accumulation of LC3B-II and p62/SQSTM1, compared to its precursors and other macrolides including roxithromycin and clarithromycin. Notably, oxidation of AZM to AZM-[O] significantly alleviated this inhibitory effect on autophagy without completely preserving its antimicrobial and immunomodulatory functions.

Conclusion: The off-target and potent block of autophagic flux demonstrated by AZM can be negated using a medicinal chemistry approach. We are currently investigating the AZM-protein interactome and further AZM derivatives that preserve the immunomodulatory function of the parent molecule, to provide a new therapeutic option for chronic respiratory disease and to safeguard the efficacy of AZM.

Short title:

Preventing Azithromycin's block of autophagy

Key words:

Airway, Antibiotic, Antibiotic tolerance, Antibiotic Resistance, Autophagy, Azithromycin, Biochemistry, Drug discovery, Epithelial, LC3, Macrolide, Medicinal Chemistry, Off-target effect, Respiratory.

Introduction

The consequences of intracellular bacteria surviving for prolonged periods in individuals who are routinely exposed to our most significant therapeutics captures some of the world's most immediate health priorities: the expansion of bacterial species that simultaneously adapt to exploit the intracellular niche and our frontline antibiotics. Accordingly, a great proportion of the world's population live for decades with respiratory conditions that require antibiotic therapy (e.g. cystic fibrosis, chronic obstructive pulmonary disease (**COPD**) and asthma). For example, despite the broad window to treat COPD, this condition remains in the top three leading cause of mortality (1, 2), and recurrent microbial infection that can reside in long-lived airway epithelial cells (**AEC**) continue to be the primary driver of disease (3-8). Moreover, macroautophagy (hereafter referred to as autophagy), which the principal mechanism responsible for clearing intracellular microbes (9), is frequently dysregulated in pulmonary disease (10, 11). Hence, the pulmonary surface in individuals with chronic respiratory disease represent a vast reservoir for bacterial adaptation (12). The convergence of these phenomena coupled with the reliance on antibiotics (to prevent a sudden increase in global mortality (13)), may be a the central reason that despite 1000's of years of pharmacological innovation (14), current therapeutic options are palliative and airway infections remain central to disease progression. Hence, it is critical to safeguard the efficacy of our frontline antibiotics in the absence of therapeutic options that target the causal mechanisms of pulmonary disease.

As for any medical intervention directed against a microbial pathogen, antibiotics can also elicit undesirable off-target effects in the mammalian cell. While it is reasonable to justify this when the off-target effects are well tolerated, a greater concern is enhancing biochemical disease mechanisms, that are beyond the sensitivity of diagnostic/clinical inquiry. A prime example of this would be blocking the host-cell's innate bacterial clearance mechanisms. We and others have found that azithromycin (**AZM**) potently blocks autophagy (4, 15, 16). Normally, in the absence of disease, bacteria are encapsulated within autophagosomes and are rapidly eliminated upon lysosomal fusion by digestive enzymes and acidic pH (9). Indeed, the consequences of perturbing the many other autophagy-mediated functions align with remarkable fidelity to the hallmark disease-related phenotypes ascribed to pulmonary disease, such as accelerated senescence (17), nutrient deprivation (18), uncontrolled autoimmune-like inflammation (19), dysfunctional cilia (20), and mitochondrial dysfunction (21). The interplay between autophagic dysregulation and respiratory disease is expansive and there have been several attempts to effectively describe their relationship (11, 22-24). One reason this off-target effect by AZM has been left unchecked is because clinical assessments of infection are confined to symptom relief, and methods in diagnostic pathology are not geared to detect intracellular bacteria. Furthermore, to our knowledge autophagy is completely disconnected from clinical and diagnostic inquiry. This points to a scenario whereby AEC are vulnerable to persistent intracellular bacteria while one of their most effective survival mechanisms is inhibited. Hence, it is important to determine how this occurs and whether AZM can be modified to maintain its efficacy and allow the cell's autophagic functions to operate normally.

AZM is a third-generation semisynthetic macrolide and is distinct from its parent molecule erythromycin A (**ERM**), due to a methyl-substituted nitrogen atom in the lactone ring ((25); and **Fig 2A**). The resulting enhanced pharmacokinetics, spectrum of activity and tolerance of AZM (vs ERM) has made it one of the world's most frequently prescribed antibiotics, which also comports with significant stewardship issues (26, 27). In part owing to its lipophilicity, AZM concentrates at the vast surface area afforded by the ciliated airway epithelium and within the airway surface liquid (25, 28). Coupled with this, AZM's physiochemical properties exhibit a remarkable capacity to passage pH and electrochemical gradients established by cellular and intracellular membranes (29). As lysosomes partition the lowest

pH environment in mammalian cells, this makes AZM extremely lysosomotropic. We and others have shown AZM accumulates in lysosomes via non-ionic diffusion at levels orders of magnitude higher than the cytosol or extracellular matrix (30-32). Aside from being sequestered from microbes in the cytosol, AZM increases lysosomal pH via ion trapping due to the protonation of two of its basic functional groups. This prohibits the normal function of lysosomal proteases, blocks autophagosome-lysosome fusion and inhibits autophagic flux with similar efficacy as bafilomycin (a widely applied inhibitor of autophagy) (4, 16). Indeed, a recent systematic review showed AZM ranked in the bottom four of nineteen antibiotics for efficacy against intracellular *S aureus* in osteomyelitis (33). What is more, the gradual leakage of AZM from lysosomes exposes bacterial communities to sub-lethal amounts of the antibiotic, enhancing their intracellular persistence (5). The importance of addressing this scenario for AZM, autophagy and chronic respiratory disease is further underscored by current concerns surrounding the paucity of new antibiotics entering the drug development pipeline (34, 35).

Given these significant challenges, we assessed the structure-activity relationship (**SAR**) of AZM vs autophagy in relation to outcomes of autophagic flux. These outcomes were also compared to other clinically relevant macrolide antibiotics and a synthesized derivative of AZM designed to counter its protonation in the lysosome (AZM-oxide, **AZM-[O]**). Outcomes for autophagy, inflammation, and bacterial growth were assessed in models of the human airway.

Methods

Clinical sampling and ethics

Ethics approval to perform airway brushings was obtained from the Central Adelaide Local Health Network Human Research Ethics Committee. Methods were conducted in accordance with the Declaration of Helsinki and with the understanding and the written consent of each participant. Airway brushing was performed by the physicians at the Royal Adelaide Hospital's Department of Thoracic Medicine. Bronchial samples were obtained from consenting control participants with no history of chronic respiratory disease and were never smokers and inpatient participants with doctor diagnosed and spirometry consistent with COPD (**Table 1**). Human primary bronchial epithelial cells were obtained from the right main bronchi using catheter brush inserted into a camera guided bronchoscope.

Cell culture

16HBE14o- (human bronchial airway epithelial cells) were purchased from EMD Millipore Corporation (Temecula, CA, USA), and propagated as per the manufacturers' instructions. Culture flasks were coated with human fibronectin (10 µg/ml), bovine serum albumin (Fraction V Stock, 100 µg/ml), and PureCol (collagen, 30 µg/ml) suspended in α-MEM (each Sigma-Aldrich, MI, USA). 16HBE14o- expansion media was α-MEM (Sigma) supplemented to 10% with fetal calf serum, 1x penicillin/streptomycin and 2 mM L-glutamine (GlutaMAX; each Thermo Fischer Scientific, MA, USA). Cells were grown in standard mammalian cell culture conditions at 37°C and 5% CO_2, with humidity. Endpoint culture formats were 12-well plates (Corning, NY, USA), seeded with $2x10^5$ cells/well in 2 ml of growth media.

The **THP-1** peripheral blood monocyte cell line was purchased from the American Type Culture Collection (Manassas, VA, USA). Growth and differentiation conditions were as previously described (36), with modifications to support conditions that approximate the proteomic profile observed in human macrophages (37). Standard mammalian cell culture conditions were used (37°C and 5% CO2, with humidity), and cells maintained in RPMI 1640 supplemented

with 50 µM ß-mercaptoethanol (both Sigma-Aldrich), 10% fetal calf serum, 1x penicillin/streptomycin and 2 mM L-glutamine (as above). Macrophage differentiation was performed for $2x10^5$ cells/well (12-well plate format), by supplementing the growth media with 50 ng/ml phorbol-12-myristate-13-acetate (PMA, Sigma-Aldrich) for 16 h, followed by a 48 h rest period.

The cell models were exposed to azithromycin-3'-N-oxide (AZM-[O]; prepared as described previously (38), solithromycin (Cayman Chemicals, MI, USA), erythromycin, telithromycin, roxithromycin, clarithromycin (Sigma-Aldrich), Erythromycin A Oxime and Erythromycin A 9,11-Imino Ether (Toronto Research Chemicals, ON, Canada), suspended in molecular biology grade dimethyl sulfoxide (DMSO, Sigma-Aldrich) less than 0.1% v/v in media. Chemical drawings were generated using ChemDraw v23.0 (PerkinElmer, MA, USA). Lipopolysaccharide (Sigma-Aldrich) was suspended in ultra-pure water.

Reverse transcription qPCR array analysis.

Quantitative reverse transcription real-time PCR (qPCR) was performed as previously described (Deholve et al., 2022). Briefly, qPCR was applied to measure transcript abundance in bronchial airway samples. RNA was extracted and genomic DNA eliminated using the RNeasy Plus column system following the manufacturers protocol (QIAGEN, Chadstone, VIC Australia). RNA was quantified using the NanoDrop One spectrophotometer (Thermo Scientific). A second gDNA purification was coupled with reverse transcription of RNA (1 µg) into cDNA with the SuperScript IV VILO ezDNase system (Thermo Scientific) using an Eppendorf Mastercycler (Eppendorf, Hamburg, Germany). cDNA samples were entered into a custom TaqMan low density array (Thermo Fisher Scientific Australia, Scoresby, VIC, Australia). qPCR was performed using 500 ng cDNA, TaqMan primer/probes technology in conjunction and TaqMan Fast Advanced Master Mix chemistry (all Thermo Scientific). The ViiA7 7300 Real Time polymerase chain reaction platform (Applied Biosystems, Carlsbad, California, USA), was used to perform qPCR. Internal reference genes (n=3) to normalise outcomes across the experimental groups were: *RNA18S5* (Hs99999901_s1), *HMBS* (Hs00609297_m1) and *TBP* (Hs00427620_m1). The primer/probes are provided in **Supplementary Table S1**.

Western blot

Western blots were performed as previously described (39). Protein was isolated using M-PER Mammalian Protein Extraction Reagent (Thermo Fisher Scientific), and Halt Protease and Phosphatase Inhibitor Cocktail (Thermo Fisher Scientific). Protein was quantified using the Pierce BCA Protein Assay Kit (Thermo Fisher Scientific), and 10 µg electrophoresed in 4–12% Bis-Tris denaturing gels (Thermo Fisher Scientific) using MOPS buffer chemistry (Thermo Fisher Scientific). Transfer was to 0.2 µm pore PVDF membranes (Bio-Rad Laboratories, CA, USA), which were sectioned so corresponding target and normalization signals could be quantified from the same blot (i.e. to mitigate loading inconsistencies due to inter-experimental variation). Membranes were blocked in 5% skim milk for mouse anti-Actin-β (1:10,000, Sigma-Aldrich, #A1978), rabbit anti-ATG5 (1:2000, AbCam, Cambridge, UK, #ab108327), rabbit anti-Poly-(ADP-ribose) polymerase (1:3,000, Cell Signaling Technology, Danvers, MS, USA, #9542), mouse anti-NRB1 (1:500, Thermo Fisher Scientific, # H00004077), and rabbit anti-Optineurin (1:2000, Cell Signaling Technology, #58981). Blocking with 5% bovine serum albumin (Merck, 126575) was used for rabbit anti-LC3B-I/II (1:3000, Cell Signaling Technology, #4108), rabbit anti-p62/Seqestosome-1 (1:3000, Cell Signaling Technology, #5114), rabbit anti-TAX1BP1 (1:2000, Cell Signaling Technology, #5105), rabbit anti-NDP52 (1:4000, Cell Signaling Technology, #60732), rabbit anti-$pMTOR^{2448}$ (1:1000, Invitrogen, MA, USA, # 441125G), rabbit anti-GATA-1 (1:1000, Cell

Signaling Technology, #3535), rabbit anti-SIRT-1 (1:100, AbCam, #ab7343), and rabbit anti-Rubicon (1:1000, Cell Signaling Technology, #8465). Membranes were subsequently probed overnight at 4°C with the same respective buffer/antibodies combinations. Secondary incubation was 1 hour at RT in 5% skim milk with mouse or rabbit IgG horseradish peroxidase-conjugated antibodies (R&D Systems, MN, USA, #HAF007 and #HAF008, respectively). The suspension for blocking and antibody incubations was 1x Tris buffered saline (Thermo Fisher Scientific), with 0.1% Tween 20 (Merck). Where possible, outcomes were derived from a single transfer membrane for the respective replicate experiments to minimise inconsistencies produced by inter-blot variation. Chemiluminescent signal production was with Amersham ECL Advanced Western Blotting Detection reagents (GE Healthcare, IL, USA). Image acquisition was performed using the LAS-4000 Luminescent Image Analyzer (Fujifilm Life Sciences, Japan), with signal detection set to annotate blots beyond the linear range (depicted by pink-purple colour). Histogram densitometry was performed using Multi Gauge software (Fujifilm Life Sciences, V3.1, Japan).

Quantification of secreted IL-6

IL-6 secretion from THP-1-derived macrophages was quantified in the growth media using enzyme-linked immunosorbent assay (ELISA; Invitrogen, #BMS213INST) following the manufacturer's protocol.

Quantification of minimum inhibitory concentration (MIC)

Assessment of MIC was conducted as previously described (Guo et al., 2023), and in accordance with the Clinical and Laboratory Standards Institute guidelines (40). Briefly, log phase (OD 0.3-0.5, 600 nm) Methicillin Sensitive *Staphylococcus aureus* (MSSA; ATCC 25923) was diluted in Mueller Hinton Broth to an optical density of 0.25 (5 x 10^5 CFU/well) and added to 96-well plates containing a two-fold concentration gradient of antibiotics (0-128 µg/ml). Cultures were exposed for 18 hours at 37°C and cell growth quantified (OD 630 nm; t_{16}-t_0 h background subtraction), in a 96-well plate reader (BioTek, Potton Bedfordshire, UK).

Statistical Methods

A Bayesian gamma (log link) generalised linear mixed model (**GLMM**) was applied (for the respective experiments/outcomes), to account for individual random effects for each sample, and target specific variances. For the transcript analysis, qPCR data was incorporated into a single multi-gene model and multi-gene normalisation was performed with the endogenous controls *18S rRNA*, hydroxymethylbilane synthase (*HMBS*) and TATA-box binding protein (*TBP*). Results were expressed as log2(Relative Expression). For each protein, Western blot densitometry results were analysed with a random effect of test repetition and reported relative to the abundance of Actin-β. For the bacterial growth assay, effects of AZM and AZM-[O] on MIC, at each antibiotic concentration, were evaluated. To assess the anti-inflammatory potential of AZM-[O], the effect of treatment*exposure-time interaction on IL-6 secretion was assessed using GLMMs with measurement timepoint (hours) included as a repeated measure. Separate analyses were performed for the 1 and 10 ng/ml LPS-stimulated THP-1 macrophage models. Statistical analyses were performed using R (v 4.0.5) for the qPCR outcomes and IBM SPSS (v28.0.1.0) for the Western blot, MIC, and IL-6 secretion data.

Results

COPD exhibits a transcript profile indicative of autophagic insufficiency.

Clinically derived COPD and control bronchial biopsies (participant demographics shown in **Table 1**) were compared for the relative activity of autophagy regulatory and effector genes and transcript markers of airway inflammation. Of note, the variability (around the observed effect size) of the autophagy transcripts displayed remarkable stability across the study groups, particularly compared to the various inflammatory markers (**Fig 1**). Delineating between the study groups, the abundance of autophagy-related transcripts showed a tendency for significant down-regulation in the COPD group vs the outcomes for the controls. Most notably, the transcription factor *GATA1*, an influential driver of autophagy gene activity exhibited a 7.69-fold reduction for the COPD cohort ($P<0.001$, vs controls). With the notable exceptions of a reduction in *TSLP* (-4.00-fold vs controls; $P=0.001$), and a trend for less *IL33* (-1.75-fold vs controls; $P=0.067$), the outcomes for inflammation were consistent with a transcript profile for epithelial cells in the context of COPD. Further to this, up-regulation of *ICAM-1* expression is concordant with a chronic injury phenotype and heightened microbial surveillance that is observed in the COPD airway. Hence, these outcomes support a scenario of autophagic dysregulation at an airway epithelium managing exogenous COPD-related exposures (e.g. the factors in cigarette smoke) and chronic inflammation in the pulmonary tissues. It is noteworthy therefore that AZM, which is routinely prescribed to manage COPD, is a poorly recognised yet potent inhibitor of autophagy.

Table 1: Participant Demographics

Study Group	Gender	Age	FEV1/FVC (%)
Control	M	62	93
	M	38	104
	M	49	94
	M	42	93
	F	51	85
	F	58	88
COPD	M	71	46
	F	65	64
	M	63	52
	F	63	67
	M	59	71
	M	53	62
	F	60	58
	F	51	66
	M	62	63

The structural modifications required to synthesize azithromycin from erythromycin inhibit autophagy.

We tracked the structure activity relationship of AZM vs autophagy, in addition to the compounds involved in the synthetic steps to produce AZM from ERM (two intervening intermediate compound ERM-9-oxime and ERM A 9,11 imino ether; **Fig 2A**). Using the abundance of LC3B-II and p62/SQSTM1 as a readout of autophagic flux, we observe a concomitant and progressive increase in LC3B-II/p62SQSTM1 signal from ERM, EM-oxime, ERM A 9,11 imino ether, and finally AZM. AZM demonstrated the largest effect size for autophagic blockade (i.e. accumulation of LC3B-II +30.7-fold, $P<0.001$ and p62/SQSTM1 +6.8-fold, $P<0.001$, vs control; **Fig 2B-C**). In support of this outcome, our

early observations show that chemical inhibitors of the mTORC complex (Ku-00063796 and Torin-1) can counter the off-target block of autophagy caused by AZM (**Supp Fig 1**). Further, tracking our fluorescently labelled AZM analogue (9a-NBD-azithromycin (31)) in 16HBE14o- cells treated with Ku-00063796 show that this outcome is associated with a redistribution of lysosomal from the perinuclear region to the periphery of the cell (**Supp Fig 2**). CLM, ROX and TLM (also semisynthetic macrolides produced from ERM), elicited a similar, albeit less pronounced accumulation of LC3B-II and p62/SQSTM1 (vs AZM). Observations during routine microscopy showed that each culture/exposure was morphologically comparable to the control, suggesting toxicity was not an obvious contributor to the outcomes for autophagy. For AZM, this was supported by non-significant outcomes for the abundance of cleaved PARP (i.e. caspase-3 activity), while the abundance of cleaved PARP due to the other (clinical) macrolides were marginally higher than background levels of programmed cell turnover. An exception was SLM (a fourth-generation pre-clinical macrolide), which caused significant cell death and detachment (PARP +2.52-fold, P=0.003). The disproportionately high pro-apoptotic effect elicited by SLM is not fully comported here due to signal-loss of cleaved PARP as a result of cell detachment. This is evidenced by a large reduction in its corresponding Actin-β signal (3.23-fold lower than the average Actin-β signal of the other exposures; P<0.001). Only Rubicon and SIRT-1, which have roles in the positive regulation of programmed cell death produced detectable/consistent signals for the SLM exposure. Notably, and excluding outcomes for SLM, while the expression of LC3B-II and p62/SQSTM1 (effectors of autophagy) demonstrated significant signal modulation (vs the control exposure), expression of the upstream pro-autophagy factors p-mTOR^{S2448}, Rubicon, SIRT1 and ATG5, were not significantly influenced by either macrolide in the context of this model. Also of note, probing p-mTOR^{S2448} in 16HBE14o- lysates provided two distinct signals of equivalent intensity, at 250 and 288 kDa. Hence, we designated both "p-mTOR^{S2448}" because, 1) both are confirmed by the manufacturer (albeit using different cell lysates), 2) related studies (to our knowledge) only report one or the other signal, 3) and, in any event, we did not observe signal modulation for p-mTOR^{S2448} using the exposures applied here.

Azithromycin causes the accumulation of autophagy receptors NBR1 and TAX1BP1 to a greater degree than Optineurin and NDP52.

The various autophagy receptor proteins exhibit differential regulation and target specificity (e.g. depolarised mitochondria or intracellular microbes). Hence, we examined Neighbor of BRCA1 gene (**NBR1**), TAX1BP1 (**TAX**), Optineurin, and Nuclear dot protein 52 (**NDP52**), to identify any differential responses to the macrolides, and vs observations for p62/SQSTM1. For the treatments in the chemical synthetic pathway from ERM to AZM, the effect size for NRB1 and TAX were strongly influenced by AZM (NBR1 +4.66-fold, P<0.001; TAX1BP1+8.68-fold, P<0.001; AZM vs control signal; **Fig 3A-B**). Interestingly for NBR1 (and to a lesser extent TAX1BP1; but distinct to the progressive elevation pattern seen in **Fig 2B** for p62/SQSTM1), the elevation in this particular autophagy receptor was confined to the influences imparted by AZM and CLM, while neither of ERM, EM-oxime, ERM A 9,11 imino ether significantly modulated NRB1 (vs the control exposure). In comparison, the abundance of Optineurin and NDP52 remained relatively consistent across each condition, including for the other semisynthetic macrolides CLM, ROX and TLM. Indeed, the most significant influence imparted by CLM, ROX and TLM (when compared to all others) was the upregulation of NBR1. Of note however (and observed for the first time to our understanding), AZM was not the most influential exposure; CLM had a greater effect for NBR1, and each of CLM, ROX and TLM increased Optineurin beyond those observed with AZM (albeit, neither were significantly larger). Given that the previous outcomes for SLM align with programmed cell death (**Fig 2B-C**), its influence here for the autophagy receptors (i.e. depletion of a stable/detectable signal), suggests NBR1, TAX1BP1, Optineurin and NDP52 do not participate in the positive regulation

of apoptosis in the context of this model (at least, as this relates to modulation of their expression levels). Taken together, these outcomes support a salient effect of AZM to prolong (and thereby increase the abundance) the duration of autophagy receptors other than p62/SQSTM1within the cell (vs basal conditions in untreated cells). This this effect is at least matched by other clinically relevant macrolides for particular autophagy receptors.

Modification of AZM charged state significantly reduces its arrest of autophagy.

One mechanism for AZM inhibition of autophagy is entry into lysosomes and increasing the pH. Amine groups of the sugar moieties give AZM a positive charge (protonated at physiological pH), that enable the lysosomotropic effect. Hence, we synthesised AZM-[O] by oxidising the desosaminyl amine which has a net alkaline pH (pKa ~ 8.1, (28)), thereby eliminating its ability to become protonated and therefore reducing the overall net charge of the molecule vs AZM (**Fig 4A**). At the highest test concentration (50 µg/ml), neutralisation of the desosaminyl amine appreciably lower the accumulation of both LC3B-II and p62/SQSTM1 in 16HBE14o- cells (AZM-[O] vs AZM, -22.07-fold and -2.88-fold, respectively, both $P<0.001$; **Fig 4B-C**). Examining the dose titration, both compounds elicited similar effects for the accumulation LC3B-II and p62/SQSTM1 for the 2.5 µg/ml intervention but became distinct at five times this amount (10 µg/ml, $P>0.05$). Of note, here the observations for cleaved PARP (apoptosis induction) grouped to produce an overall elevated outcome (vs outcomes in **Fig 2**), for 10 and 50 µg/ml of AZM (2.31-fold, $P=0.004$ and 3.961-fold, $P<0.001$, respectively, vs control). While this agrees with inhibiting the pro-survival influences imparted by autophagy, routine microscopic observations showed the cells were not morphologically distinct from the control exposure.

Oxidation of the AZM desosaminyl amine reduces its bacteriostatic activity.

We assessed the minimum inhibitory concentration (**MIC**) for dose titrations of AZM and AZM-[O] to determine whether the oxidation of AZM desosaminyl amine modulate its bacteriostatic activity. Shown in **Fig 5**, AZM has exceptionally effective bacteriostatic activity, inhibiting the growth of methicillin sensitive *Staphylococcus aureus* (**MSSA**) at an MIC within 1-4 µg/ml. In contrast the antimicrobial activity of AZM-[O] was significantly attenuated and was only able to affect a bacteriostatic outcome at the maximum exposure of 128 µg/ml. This outcome is consistent with an essential function of the AZM sugar amine moieties (here for the desosaminyl amine) as important structural determinants that enables its inhibition of the bacterial 50S ribosomal subunit.

AZM-[O] exhibits attenuated anti-inflammatory properties vs AZM.

One beneficial off-target influence imparted by AZM is a moderate anti-inflammatory effect. To determine whether AZM-[O] retained this anti-inflammatory property, we quantified the magnitude of secreted IL-6 in an LPS-stimulated THP-1 macrophage model, co-exposed to either AZM or AZM-[O]. AZM significantly moderated the secretion of IL-6 when THP-1 macrophages were treated with 1 ng/ml LPS for the 6 and 24 hour exposure intervals (-95.80 ng/ml, $P<0.001$ and -86.19 ng/ml, $P=0.002$, vs control, respectively; **Fig 6A**), while AZM-[O] elicited a similar, albeit less influential effect (-22.55 ng/ml, $P<0.04$ and -55.37 ng/ml, $P=0.04$, vs control, respectively). In contrast, outcomes for AZM-[O] with 10 ng/ml LPS for either time interval were indiscernible from the control exposure (**Fig 6B**). Interestingly, AZM was also less effective in the 10 ng/ml LPS model, with a significant outcome for the 6 hour LPS exposure (-130.43 ng/ml, $P<0.001$, vs control), but a non-significant result for the 24 h model (-62.9 ng/ml, $P=0.161$, vs control). That AZM was also relatively less effective for the 24 hour interval with 1 ng/ml LPS (vs the 6 hour interval), hints to a washout mechanism possibly related to chemical stability within the cell the turnover of organelles containing AZM.

Discussion

There is an emerging medical crisis due to bacteria becoming resilient to our frontline antibiotics. This problem is coupled with an apparent lack of urgency to develop new antibiotics to address this issue (35). AZM is exceptionally effective, but there are increasing calls to develop regulatory regimes to combat the emergence of AZM tolerance species (e.g. (41)). Given these issues, it is surprising that there is a relative paucity of information that describes AZM's potent off-target inhibition of autophagy – a fundamental survival process that also serves as the cells' most effective bacterial clearance mechanism.

Here, we provide evidence that factors regulating autophagy are intrinsically downregulated in COPD and demonstrate that AZM potently inhibits autophagy in human airway models. We also show that targeting its charged state (AZM-[O]) is one method to overcome this off-target effect, and that the desosaminyl amine is a structural determinant for AZM's antibacterial and anti-inflammatory activity.

While AZM-[O] effectively addressed the off-target inhibition of autophagy, this structural modification (oxidation of the desosaminyl amine) diminished the antibacterial and anti-inflammatory activity exhibited by the parent molecule. An ideal outcome would be a non-antibiotic form of AZM, which mitigates the off-target arrest of autophagy and retains its immunomodulatory properties. Such a derivative would provide an invaluable non-steroidal anti-inflammatory that concentrates at the airways, without contributing to the selection of AZM-resistance bacteria (42). This has been examined by Kragol et al. (2022), who synthesised a stereoisomer of AZM with immunomodulatory activity, although there was no further assessment to determine whether the suppressive effects on autophagy were altered (43). Indeed, given the wide use of AZM and its remarkable capacity to localise within the mammalian cell, surprisingly little research been conducted to identify further off-target effects. Even its unique anti-inflammatory properties, which may provide mechanistic leads for new immunomodulatory options, await a clear description (44). For autophagy, AZM-mTOR interactions (via inhibition of S6RP phosphorylation) have been described in the context of idiopathic bronchiolitis, albeit using a high concentration of AZM (300 ug/ml) and a direct interaction was not identified (45). No studies have attempted to identify specific lysosomal ion channel or transporter binding domains that could inform SAR studies to address AZM-mediated suppression of autophagosome-lysosome fusion.

To address these gaps, we are developing an AZM-diazirine photoaffinity probe to identify proteins that photocross-link with AZM. The outcomes will be to be used to 1) map the AZM-protein interactome in models of the human airway epithelium, 2) inform the development of further AZM-derivatives, and 3) functionally validate the derivatives that mitigate the arrest of autophagy and that exhibit immunomodulatory effects observed for the parent molecule. It is our hope that outcomes from this inquiry will and provide new treatment options for COPD and safeguard AZM for future clinical application.

Acknowledgements

We are grateful for the expertise and support of the clinical staff of the Royal Adelaide Hospital Thoracic Department, The Queen Elizabeth Hospital Respiratory Unit and the participants enrolled into this study who generously provided their valuable time and tissue samples. We are also thankful for the pharmacological insight provided by Prof Benedetta Sallustio (University of Adelaide) and assistance in chemical synthesis by Christian Danker (University of South Australia). This study was funded by the Royal Adelaide Research Committee, Royal Adelaide Hospital Research Fund, The Health Services Charitable Gifts Board, and the Rebecca L Cooper Medical Research Foundation.

Disclosure statement.

The authors have no COI to disclose.

Figure legends.

Figure 1: Autophagy gene activity is reduced in COPD.

Transcript abundance of key positive regulators of autophagy are downregulated in COPD (n=9, age 60.8 ±SD 6.06, FEV1/FVC 64.5 ±SD 4.51) vs controls (n=6, age 50.0 ±9.14 SD, FEV1/FVC 92.83 ±6.49 SD) bronchial brushing biopsies. With some exceptions (notably *TSLP* and *IL-33*), these changes associated with an upregulation of inflammatory and cell adhesion transcripts. Magnitudes are expressed as COPD vs control (i.e. less/more transcript abundance in COPD-derived samples to the left/right of zero, respectively), and ordered to highlight transcript groups related to gene-dependent variation. Dashed vertical lines for log2(relative expression) at – 2.0 correspond to a fold-change of 0.25, and + 2.0 correspond to a fold-change of 4.0. Results are normalised to three reference genes and are significant to at least $P<0.05$ when 95% CI do not cross zero.

Figure 2: Azithromycin causes a heightened autophagic arrest response in human airway epithelial cells compared to its precursor compounds and related macrolide antibiotics.

A. Comparative chemical structure of the macrolides. The lactone macrocyclic ring (numbering indicates carbon/nitrogen bonds) is bonded with a desosamine sugar group (upper five carbon ring moiety bound through AZM C5) for each antibiotic and the cladinose sugar (lower five carbon ring moiety bound through AZM C3) for each except TEL and SOL. **B.** 16HBE14o- cell responses to the macrolide exposures. Outcomes represent n=3 independent cultures/Western blots. Outcomes for the target proteins that demonstrated significant response/modulation to the exposure(s) are shown. Outcomes for each of the respective n=3 repeated measures of the targets were derived from a single transfer membrane to minimise inconsistencies produced by inter-blot variation. Expressions was normalized to Actin-β. Effect sizes represented fold-change relative to the control treatment and uncertainty intervals are ± 95% CI. Results are significant to at least $P<0.05$ when 95% CI do not cross the dashed line (1-fold). Vehicle (VEH) is ≤ 0.1% DMSO vs culture volume. **C.** Western blot showing protein signals derived from the 16HBE14o- model exposed to the various macrolides (16 h, 50 µg/ml). Large and concomitant increase in LC3B-II and p62/SQSTM1 abundance for the AZM exposure (vs control), indicates a heightened arrest of autophagic flux (i.e. reduced autolysosomal turnover). This effect appears to be independent of alteration in protein abundance of influential up-stream pro-autophagy factors such as p-mTOR^{S2448} and SIRT1.

Figure 3: The autophagy receptors NBR1 and TA1BP1 are elevated by Azithromycin.

A. Quantification of the protein abundance measures for the autophagy receptors NBR1, TAX1BP1, Optineurin and NDP52 in 16HBE14o- cell exposed to the macrolides (16 h, 50 µg/ml). Effect sizes represent n=3 independent cultures/Western blots. Outcomes for each of the respective repeated measures of the targets were derived from a single transfer membrane to minimise inconsistencies produced by inter-blot variation. Expressions was normalised to Actin-β. Effect sizes represented fold-change relative to the control treatment and uncertainty intervals are ±95% CI. Results are significant to at least $P<0.05$ when 95% CI do not cross the dashed line (1-fold). **B.** Western blot shows autophagy receptor protein signals from 16HBE14o- cultures exposed to the various macrolides (16 h, 50 µg/ml). Responses for NBR1 and TAX1BP1 show significant signal modulation when the 16HBE14o- cells were exposed to AZM, but relatively less Optineurin and NDP52 was observed to accumulate as a result of this macrolide (vs the control exposure). Interestingly, CLM elicited a stronger (but not statistically distinct) effect for the elevation of NBR1 vs AZM, and each of CLM, ROX and TLM produced a similar outcome (vs AZM) for the autophagy receptor Optineurin.

Figure 4: Structure-activity relationship of AZM vs autophagy shows oxidation of the desosaminyl amine diminishes its off-target block of autophagy.

A. Perspective formula representation of AZM showing the oxidation of the desosaminyl amine. Addition of the oxide produces a zwitterionic group (no net charge) to the desosaminyl amine (blue circles), to block protonation of the amine group. **B.** Quantification of the outcomes of Western blot analyses shows the concomitant increase in the abundance of LC3B-II and p62/SQSTM1 for AZM is significantly reduced for the AZM-[O] derivative. The outcomes for AZM and LC3B-II / p62/SQSTM1 follow a dose relationship (2.5, 10, and 50 µg/ml; 16 h). Here, this outcome is matched by a progressive increase in apoptosis with AZM (as assess via the abundance of cleaved PARP), which is not observed after exposure with the oxidised form. Expressions was normalised to Actin-β. Effect sizes represented fold-change relative to the control treatment and uncertainty intervals are ±95% CI. Results are significant to at least $P<0.05$ when 95% CI do not cross the dashed line (1-fold). **C.** Representative Western blot shows the processing of PARP to produce cleaved PARP, and the concomitant increase in LC3B-II and p62/SQSTM1 progressively increases in 16HBE14o- cells after stimulation with AZM, but which is not observed for AZM-[O]. Actin-β served as the loading control.

Figure 4: AZM-[O] exhibits low bacteriostatic efficacy vs the AM parent molecule.

MSSA was used to model the comparative bacteriostatic potential of AZM vs the AZM-[O] derivative. Whereas AZM has is extremely effective in preventing the growth of MSSA (MIC of approximately 2 µg/ml over a 16 hour assay period), AZM-[O] approached MIC at the maximum dose of 128 µg/ml (over 64-fold reduction in bacteriostatic activity vs AZM). The bacteriostatic effect of AZM-[O] was approximately 105% lower than AZM at every exposure dose ($P<0.001$). Outcomes represent n=7 replicate experiments; shaded area represents ±SD.

Figure 6: Oxidation of AZM desosaminyl amine attenuates its anti-inflammatory activity.

The secretion of IL-6 was used to assess the anti-inflammatory effect imparted by AZM vs. AZM-[O]. THP-1 macrophages stimulated with LPS respond by secreting IL-6 into the media, particularly for the 6 and 24 hour time period. AZM reduction of IL-6 was most evident after co-exposure with 1 ng/ml LPS for the 6 and 24 hour treatment intervals, and to a similar extend for 10 ng/ml LPS after 6 hours. In contrast, AZM-[O] exhibited a significantly attenuated effect for the reduction of secreted IL-6 (vs the parent molecule) with 1 ng/ml LPS, and outcomes using 10

ng/ml LPS were comparable to the control exposure. Outcomes represent n=3 separate experiments; confidence intervals are ±SD.

Supp Fig 1: Chemical inhibitors of mTORC1/2 can counter AZM block of autophagy.

16HBE14o- cells were exposed to 10 or 50 µg/ml AZM and increasing concentrations of the chemical blockers of mTOCR1/2, Ku-0063794 ("KU") and Torin-1 (16 hour co-treatment). Western blot outcomes show a reduction in LC3B-II and p62/SQSTM1 abundance that follows a dose relationship for increasing concentrations of the mTORC1/2 inhibitors, which is particularly evident for the 50 µg/ml AZM co-exposure model. This outcome was also noted for the autophagy receptor TAX1BP1. These outcomes suggest a partial restoration of autophagic flux by overcoming the potent block imposed by AZM. Outcomes for each respective target (representative of n=2 blots) were derived from a single transfer membrane to minimise inconsistencies produced by inter-blot variation. Actin-β served as a loading control.

Supp Fig 2: Ku-0063794 promotes redistribution of lysosomes from the perinuclear region by 9a-NBD-azithromycin to the cell periphery.

Lysosomes were loaded with 10 µg/mL the fluorescent AZM analogue 9a-NBD-AZM for 2 h in the 16HBE14o- cell model and then treated with the chemical inhibitor of mTORC1/2, Ku-0063794 (10 µM, 16 hours after exposure to 9a-NBD-AZM). Confocal immunofluorescence microscopy shows the cells treated with 9a-NBD-AZM have lysosomes localised around the nucleus. Ku-0063794 promoted the redistribution of lysosomes loaded with the fluorescent AZM analogue to the periphery of the cells. This redistribution pattern from the centre (autophagic block via 9a-NBD-AZM) to the periphery (active autophagy) is indicative of the restoration of autophagic activity. Outcomes represent n=3 independent experiments.

Reference list.

1. Syamlal G, Kurth LM, Dodd KE, Blackley DJ, Hall NB, Mazurek JM. Chronic Obstructive Pulmonary Disease Mortality by Industry and Occupation - United States, 2020. MMWR Morb Mortal Wkly Rep. 2022;71(49):1550-4.
2. Viegi G, Maio S, Fasola S, Baldacci S. Global Burden of Chronic Respiratory Diseases. J Aerosol Med Pulm Drug Deliv. 2020;33(4):171-7.
3. Ramsheh MY, Haldar K, Bafadhel M, George L, Free RC, John C, et al. Resistome analyses of sputum from COPD and healthy subjects reveals bacterial load-related prevalence of target genes. Thorax. 2020;75(1):8-16.
4. Poh WP, Kicic A, Lester SE, Nguyen PT, Bakaletz LO, Reynolds PN, et al. COPD-Related Modification to the Airway Epithelium Permits Intracellular Residence of Nontypeable Haemophilus influenzae and May Be Potentiated by Macrolide Arrest of Autophagy. Int J Chron Obstruct Pulmon Dis. 2020;15:1253-60.
5. Liu X, Liu F, Ding S, Shen J, Zhu K. Sublethal Levels of Antibiotics Promote Bacterial Persistence in Epithelial Cells. Adv Sci (Weinh). 2020;7(18):1900840.
6. Rawlins EL, Hogan BL. Ciliated epithelial cell lifespan in the mouse trachea and lung. Am J Physiol Lung Cell Mol Physiol. 2008;295(1):L231-4.
7. Sethi S, Maloney J, Grove L, Wrona C, Berenson CS. Airway inflammation and bronchial bacterial colonization in chronic obstructive pulmonary disease. Am J Respir Crit Care Med. 2006;173(9):991-8.
8. Patel IS, Seemungal TA, Wilks M, Lloyd-Owen SJ, Donaldson GC, Wedzicha JA. Relationship between bacterial colonisation and the frequency, character, and severity of COPD exacerbations. Thorax. 2002;57(9):759-64.
9. Mao K, Klionsky DJ. Xenophagy: A battlefield between host and microbe, and a possible avenue for cancer treatment. Autophagy. 2017;13(2):223-4.
10. Tan WSD, Shen HM, Wong WSF. Dysregulated autophagy in COPD: A pathogenic process to be deciphered. Pharmacol Res. 2019;144:1-7.
11. Racanelli AC, Kikkers SA, Choi AMK, Cloonan SM. Autophagy and inflammation in chronic respiratory disease. Autophagy. 2018;14(2):221-32.
12. Mina MJ, Klugman KP. The role of influenza in the severity and transmission of respiratory bacterial disease. Lancet Respir Med. 2014;2(9):750-63.
13. Gordon RJ, Gordon RJ, De G, Gordon RJ, Gordon RJ. The Rise and Fall of American Growth : The U.S. Standard of Living since the Civil War. Princeton, NJ: Princeton University Press; 2017.
14. Stein SW, Thiel CG. The History of Therapeutic Aerosols: A Chronological Review. J Aerosol Med Pulm Drug Deliv. 2017;30(1):20-41.
15. Mukai S, Moriya S, Hiramoto M, Kazama H, Kokuba H, Che XF, et al. Macrolides sensitize EGFR-TKI-induced non-apoptotic cell death via blocking autophagy flux in pancreatic cancer cell lines. Int J Oncol. 2016;48(1):45-54.
16. Renna M, Schaffner C, Brown K, Shang S, Tamayo MH, Hegyi K, et al. Azithromycin blocks autophagy and may predispose cystic fibrosis patients to mycobacterial infection. J Clin Invest. 2011;121(9):3554-63.
17. Barnes PJ, Baker J, Donnelly LE. Cellular Senescence as a Mechanism and Target in Chronic Lung Diseases. Am J Respir Crit Care Med. 2019;200(5):556-64.
18. Roscioli E, Tran HB, Jersmann H, Nguyen PT, Hopkins E, Lester S, et al. The uncoupling of autophagy and zinc homeostasis in airway epithelial cells as a fundamental contributor to COPD. Am J Physiol Lung Cell Mol Physiol. 2017;313(3):L453-L65.
19. Dong LL, Liu ZY, Chen KJ, Li ZY, Zhou JS, Shen HH, Chen ZH. The persistent inflammation in COPD: is autoimmunity the core mechanism? Eur Respir Rev. 2024;33(171).
20. Cloonan SM, Lam HC, Ryter SW, Choi AM. "Ciliophagy": The consumption of cilia components by autophagy. Autophagy. 2014;10(3):532-4.
21. Ng Kee Kwong F, Nicholson AG, Harrison CL, Hansbro PM, Adcock IM, Chung KF. Is mitochondrial dysfunction a driving mechanism linking COPD to nonsmall cell lung carcinoma? Eur Respir Rev. 2017;26(146).
22. Barnes PJ, Burney PG, Silverman EK, Celli BR, Vestbo J, Wedzicha JA, Wouters EF. Chronic obstructive pulmonary disease. Nat Rev Dis Primers. 2015;1:15076.
23. Li ZY, Wu YF, Xu XC, Zhou JS, Wang Y, Shen HH, Chen ZH. Autophagy as a double-edged sword in pulmonary epithelial injury: a review and perspective. Am J Physiol Lung Cell Mol Physiol. 2017;313(2):L207-L17.
24. Liao SX, Sun PP, Gu YH, Rao XM, Zhang LY, Ou-Yang Y. Autophagy and pulmonary disease. Ther Adv Respir Dis. 2019;13:1753466619890538.
25. Heidary M, Ebrahimi Samangani A, Kargari A, Kiani Nejad A, Yashmi I, Motahar M, et al. Mechanism of action, resistance, synergism, and clinical implications of azithromycin. J Clin Lab Anal. 2022;36(6):e24427.
26. Labi AK, Obeng-Nkrumah N, Dayie N, Egyir B, Sampane-Donkor E, Newman MJ, Opintan JA. Antimicrobial use in hospitalized patients: a multicentre point prevalence survey across seven hospitals in Ghana. JAC Antimicrob Resist. 2021;3(3):dlab087.

27. McMullan BJ, Mostaghim M. Prescribing azithromycin. Aust Prescr. 2015;38(3):87-9.
28. Laux J, Martorelli M, Strass S, Schollmeyer D, Maier F, Burnet M, Laufer SA. Inherent Fluorescence Demonstrates Immunotropic Properties for Novel Janus Kinase 3 Inhibitors. ACS Pharmacol Transl Sci. 2023;6(10):1433-52.
29. Aubert JD, Juillerat-Jeanneret L, Fioroni P, Dayer P, Plan PA, Leuenberger P. Function of human alveolar macrophages after a 3-day course of azithromycin in healthy volunteers. Pulm Pharmacol Ther. 1998;11(4):263-9.
30. Derendorf H. Excessive lysosomal ion-trapping of hydroxychloroquine and azithromycin. Int J Antimicrob Agents. 2020;55(6):106007.
31. Matijasic M, Munic Kos V, Nujic K, Cuzic S, Padovan J, Kragol G, et al. Fluorescently labeled macrolides as a tool for monitoring cellular and tissue distribution of azithromycin. Pharmacol Res. 2012;66(4):332-42.
32. Nujic K, Banjanac M, Munic V, Polancec D, Erakovic Haber V. Impairment of lysosomal functions by azithromycin and chloroquine contributes to anti-inflammatory phenotype. Cell Immunol. 2012;279(1):78-86.
33. Zelmer AR, Nelson R, Richter K, Atkins GJ. Can intracellular Staphylococcus aureus in osteomyelitis be treated using current antibiotics? A systematic review and narrative synthesis. Bone Res. 2022;10(1):53.
34. Klug DM, Idiris FIM, Blaskovich MAT, von Delft F, Dowson CG, Kirchhelle C, et al. There is no market for new antibiotics: this allows an open approach to research and development. Wellcome Open Res. 2021;6:146.
35. Piddock LJ. The crisis of no new antibiotics--what is the way forward? Lancet Infect Dis. 2012;12(3):249-53.
36. Hamon R, Tran HB, Roscioli E, Ween M, Jersmann H, Hodge S. Bushfire smoke is pro-inflammatory and suppresses macrophage phagocytic function. Sci Rep. 2018;8(1):13424.
37. Pinto SM, Kim H, Subbannayya Y, Giambelluca MS, Bosl K, Ryan L, et al. Comparative Proteomic Analysis Reveals Varying Impact on Immune Responses in Phorbol 12-Myristate-13-Acetate-Mediated THP-1 Monocyte-to-Macrophage Differentiation. Front Immunol. 2021;12:679458.
38. Codony A DJ, Garcia R, Rifa J, inventor; Sandoz AG, Basel (CH), assignee. Derivatives of azithromycin. United States2004.
39. Delhove J, Alawami M, Macowan M, Lester SE, Nguyen PT, Jersmann HPA, et al. Organotypic sinonasal airway culture systems are predictive of the mucociliary phenotype produced by bronchial airway epithelial cells. Sci Rep. 2022;12(1):19225.
40. Humphries RM, Miller L, Zimmer B, Matuschek E, Hindler JA. Contemporary Considerations for Establishing Reference Methods for Antibacterial Susceptibility Testing. J Clin Microbiol. 2023;61(6).
41. Mack I, Sharland M, Berkley JA, Klein N, Malhotra-Kumar S, Bielicki J. Antimicrobial Resistance Following Azithromycin Mass Drug Administration: Potential Surveillance Strategies to Assess Public Health Impact. Clin Infect Dis. 2020;70(7):1501-8.
42. Mencarelli A, Distrutti E, Renga B, Cipriani S, Palladino G, Booth C, et al. Development of non-antibiotic macrolide that corrects inflammation-driven immune dysfunction in models of inflammatory bowel diseases and arthritis. Eur J Pharmacol. 2011;665(1-3):29-39.
43. Kragol G, Steadman VA, Marusic Istuk Z, Cikos A, Bosnar M, Jelic D, et al. Unprecedented Epimerization of an Azithromycin Analogue: Synthesis, Structure and Biological Activity of 2'-Dehydroxy-5''-Epi-Azithromycin. Molecules. 2022;27(3).
44. Slater M, Torr E, Harrison T, Forrester D, Knox A, Shaw D, Sayers I. The differential effects of azithromycin on the airway epithelium in vitro and in vivo. Physiol Rep. 2016;4(18).
45. Weng D, Wu Q, Chen XQ, Du YK, Chen T, Li H, et al. Azithromycin treats diffuse panbronchiolitis by targeting T cells via inhibition of mTOR pathway. Biomed Pharmacother. 2019;110:440-8.

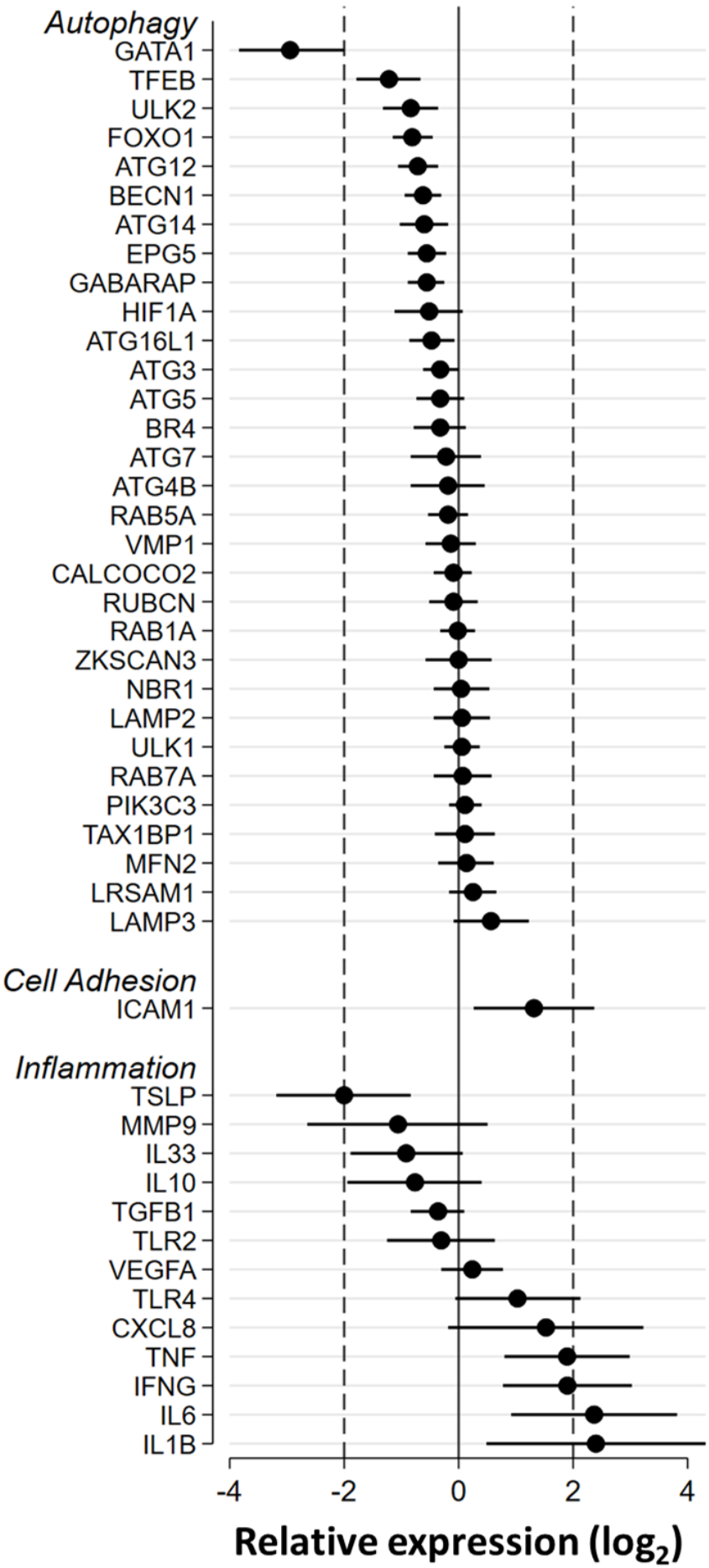
Autophagy
GATA1
TFEB
ULK2
FOXO1
ATG12
BECN1
ATG14
EPG5
GABARAP
HIF1A
ATG16L1
ATG3
ATG5
BR4
ATG7
ATG4B
RAB5A
VMP1
CALCOCO2
RUBCN
RAB1A
ZKSCAN3
NBR1
LAMP2
ULK1
RAB7A
PIK3C3
TAX1BP1
MFN2
LRSAM1
LAMP3
Cell Adhesion
ICAM1
Inflammation
TSLP
MMP9
IL33
IL10
TGFB1
TLR2
VEGFA
TLR4
CXCL8
TNF
IFNG
IL6
IL1B
-4
-2
0
2
4
Relative expression (log2)

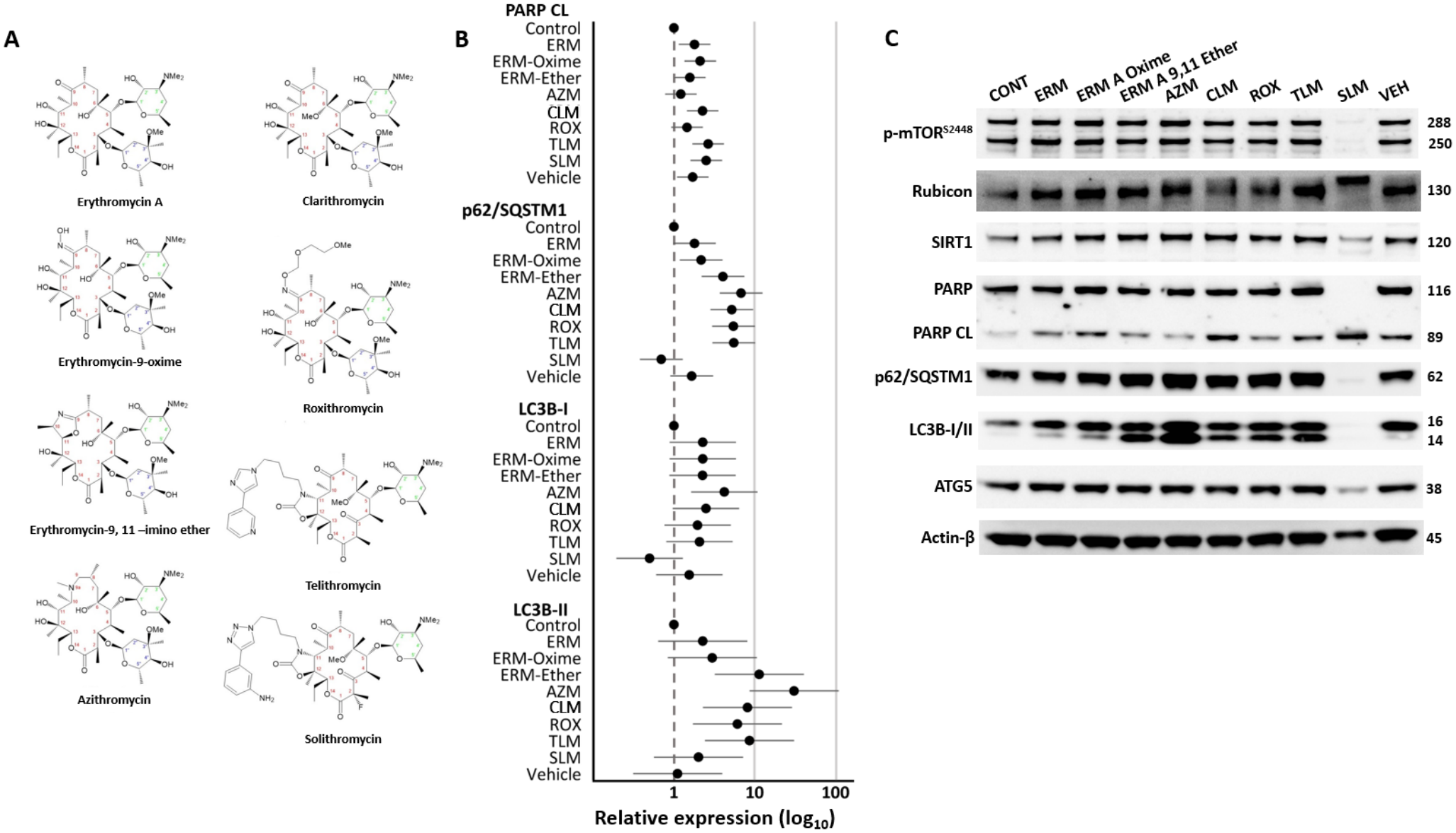
A
Erythromycin A
Clarithromycin
Erythromycin-9-oxime
Roxithromycin
Erythromycin-9, 11 –imino ether
Telithromycin
Azithromycin
Solithromycin
B
PARP CL
p62/SQSTM1
LC3B-I
LC3B-II
Control
ERM
ERM-Oxime
ERM-Ether
AZM
CLM
ROX
TLM
SLM
Vehicle
1
10
100
Relative expression (log10)
C
CONT
ERM
ERM A Oxime
ERM A 9,11 Ether
AZM
CLM
ROX
TLM
SLM
VEH
p-mTORS2448
288
250
Rubicon
130
SIRT1
120
PARP
116
PARP CL
89
p62/SQSTM1
62
LC3B-I/II
16
14
ATG5
38
Actin-β
45

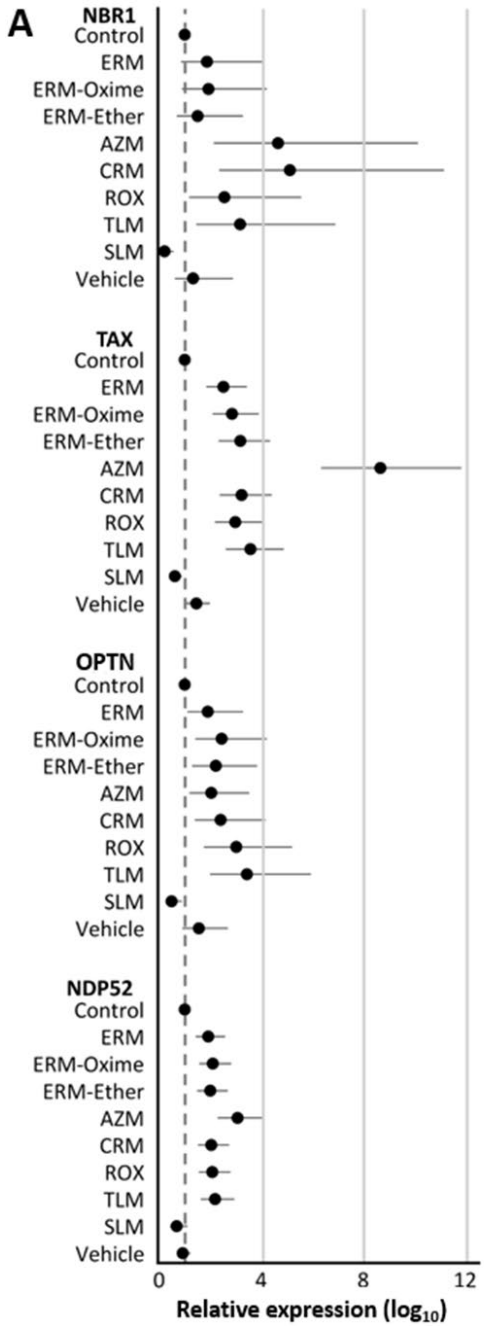
A
NBR1
Control
ERM
ERM-Oxime
ERM-Ether
AZM
CRM
ROX
TLM
SLM
Vehicle
TAX
Control
ERM
ERM-Oxime
ERM-Ether
AZM
CRM
ROX
TLM
SLM
Vehicle
OPTN
Control
ERM
ERM-Oxime
ERM-Ether
AZM
CRM
ROX
TLM
SLM
Vehicle
NDP52
Control
ERM
ERM-Oxime
ERM-Ether
AZM
CRM
ROX
TLM
SLM
Vehicle
0
4
8
12
Relative expression (log10)

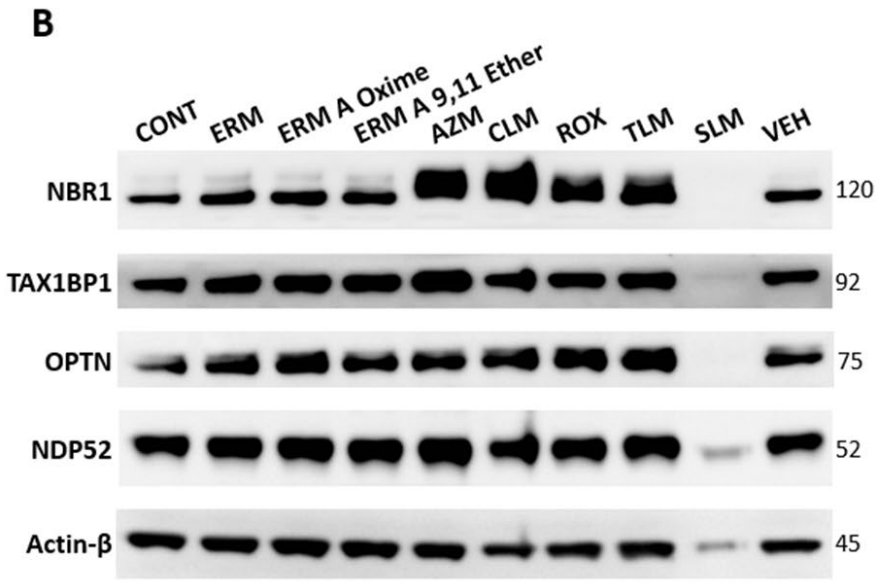
B
CONT
ERM
ERM A Oxime
ERM A 9,11 Ether
AZM
CLM
ROX
TLM
SLM
VEH
NBR1
120
TAX1BP1
92
OPTN
75
NDP52
52
Actin-β
45

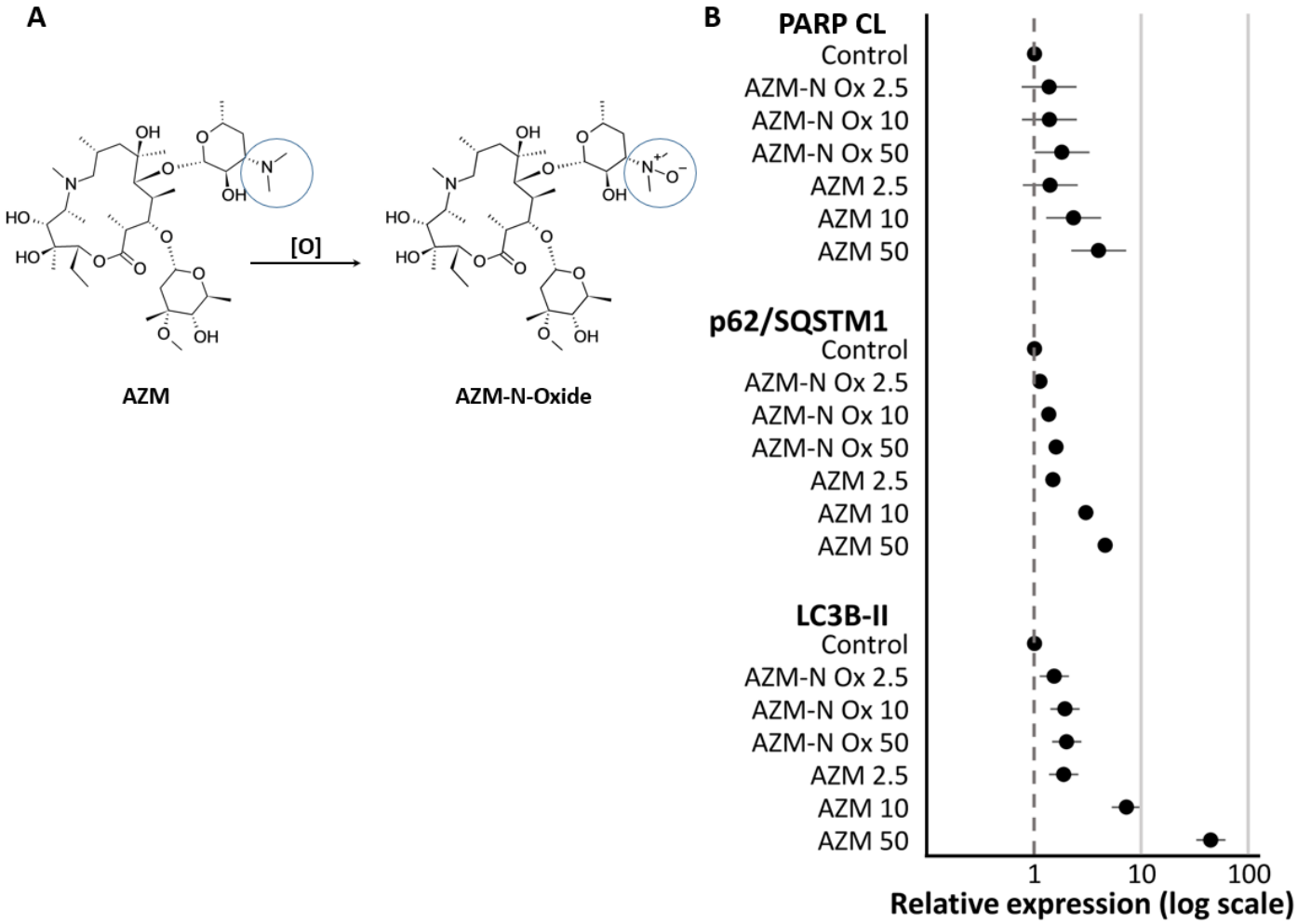
A
[O]
AZM
AZM-N-Oxide
B
PARP CL
Control
AZM-N Ox 2.5
AZM-N Ox 10
AZM-N Ox 50
AZM 2.5
AZM 10
AZM 50
p62/SQSTM1
Control
AZM-N Ox 2.5
AZM-N Ox 10
AZM-N Ox 50
AZM 2.5
AZM 10
AZM 50
LC3B-II
Control
AZM-N Ox 2.5
AZM-N Ox 10
AZM-N Ox 50
AZM 2.5
AZM 10
AZM 50
1
10
100
Relative expression (log scale)
C
CONT
AZM-N-Ox 2.5
AZM-N-Ox 10
AZM-N-Ox 50
AZM 2.5
AZM 10
AZM 50
PARP
PARP CL
p62/SQSTM1
LC3B-I/II
Actin-β
116
89
62
14
16
45

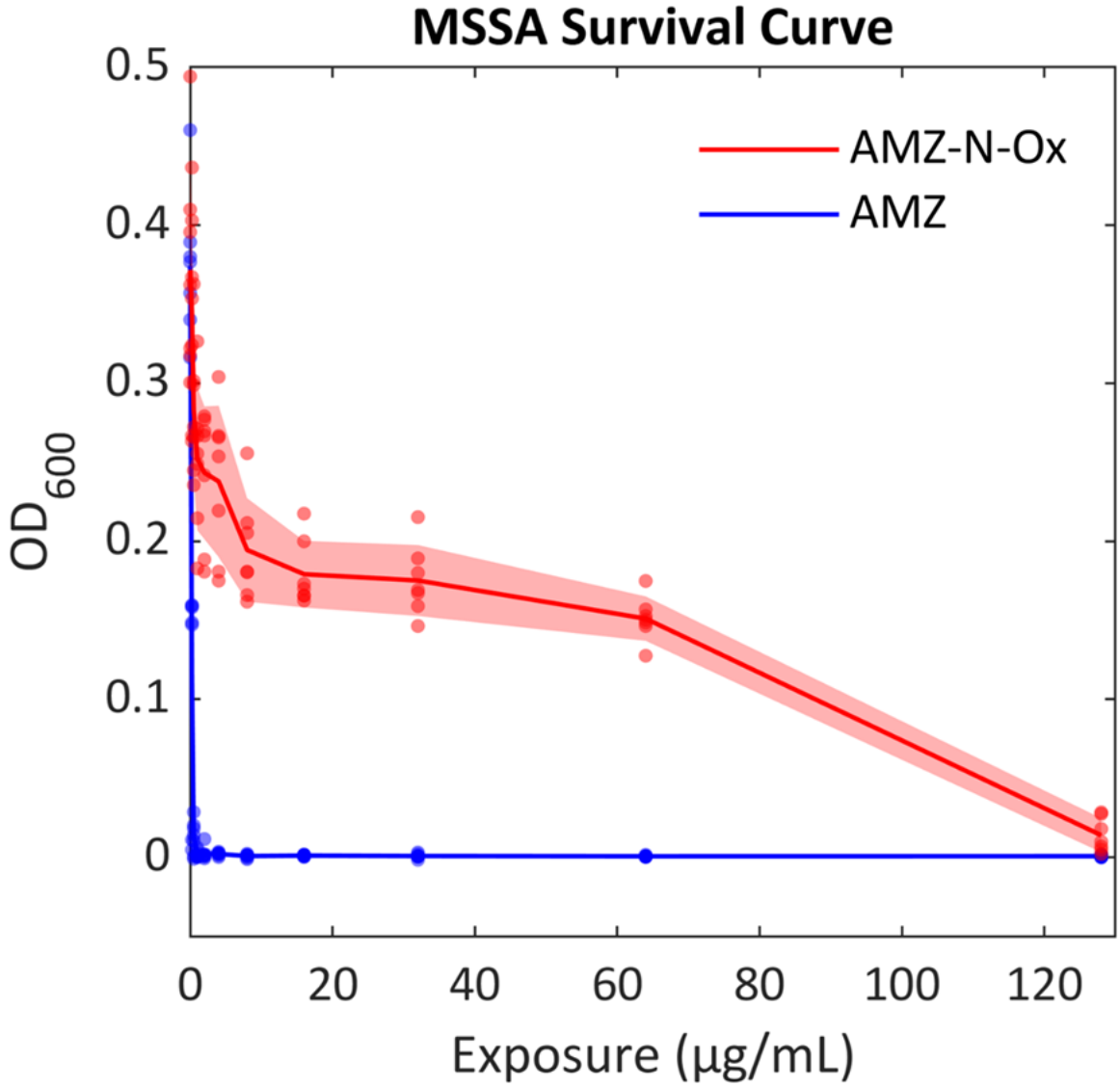
MSSA Survival Curve
AMZ-N-Ox
AMZ
OD600
0.5
0.4
0.3
0.2
0.1
0
0
20
40
60
80
100
120
Exposure (µg/mL)

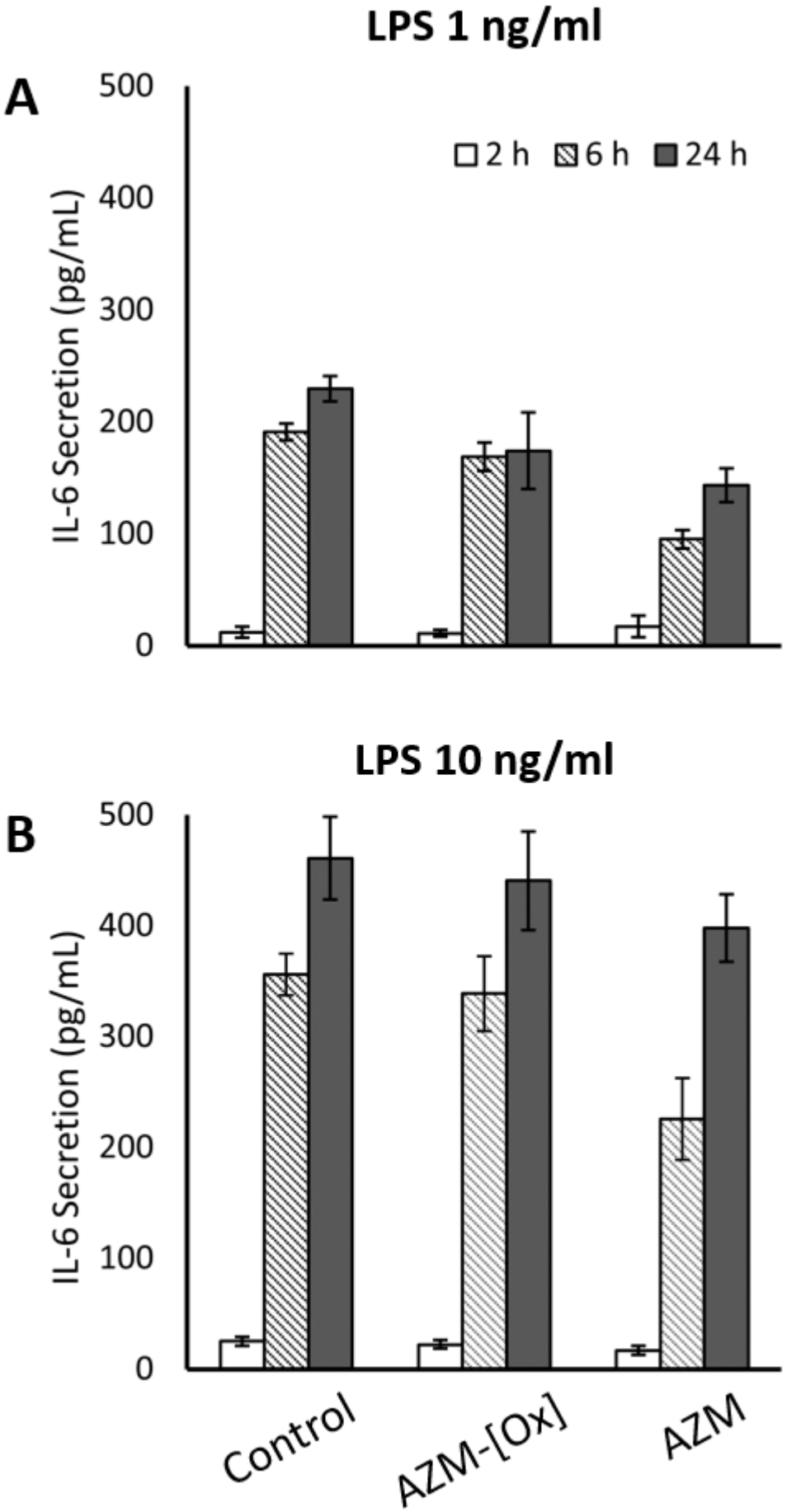
LPS 1 ng/ml
A
500
400
300
200
100
0
IL-6 Secretion (pg/mL)
2 h
6 h
24 h
LPS 10 ng/ml
B
500
400
300
200
100
0
IL-6 Secretion (pg/mL)
Control
AZM-[Ox]
AZM